Two-dimensional higher-band vortex lattice solitons

Ofer Manela, Oren Cohen, Guy Bartal, Jason W. Fleischer, and Mordechai Segev

Department of Physics and Solid State Institute, Technion, Haifa 32000, Israel

Received March 15, 2004

We study self-localized second-band vortex states in two-dimensional photonic lattices and find stable ring solitons whose phase forms an array of counterrotating vortices. We also identify composite solitons in which a second-band vortex is jointly trapped with a mode arising from the first band and study their stability. When such a composite entity is unstable, it disintegrates while exchanging angular momentum between its constituents, eventually stabilizing into another form of composite soliton. © 2004 Optical Society of America

OCIS codes: 190.4420, 190.5940.

Wave propagation in nonlinear periodic structures exhibits many interesting phenomena.[1] The periodicity of the refractive index alters diffraction, whereas the nonlinearity leads to the creation of localized waves: lattice (discrete) solitons.[1,2] The observation of such solitons[3] has led to a surge of research on wave propagation in one-dimensional (1D) nonlinear periodic structures and to the observation of gap lattice solitons,[4] dipole mode lattice solitons,[5] high band lattice solitons,[6] and vector lattice solitons.[7] This recent progress has led to exciting ideas in two-dimensional (2D) lattices,[8] such as vortex lattice solitons,[9–11] 2D vector lattice solitons,[12] etc. Experimentally, the recent suggestion of the real-time optical induction technique[13] has allowed the first observations of 2D lattice solitons[14] and of first-band vortex lattice solitons.[15,16]

Here, we identify lattice solitons arising from the X symmetry points of the second band, residing in the gap between the first and the second bands of a square lattice, i.e., a spatial gap soliton with vorticity. Such solitons have the phase structure of a counterrotating vortex array and are stable for moderate lattice depths and soliton intensities. We also identify composite lattice solitons in which such a second-band vortex mode is jointly trapped with a mode arising from the first band. Interestingly, in regimes in which such an entity is unstable, it disintegrates while exchanging angular momentum between its constituents, eventually stabilizing into another form of composite lattice soliton.

Linear lattices show typical transmission spectra exhibiting allowed bands and forbidden gaps. In a waveguide array, a complete gap is a range of propagation constants (β) that are not associated with any propagating mode. For 1D lattices there are typically an infinite number of complete gaps, whereas in 2D lattices[14] the number of complete gaps can be small, sometimes none.[8] The higher dimensionality also leads to the existence of multiple symmetry points setting the band edges of 2D lattices, which can exhibit direct or indirect bandgaps. Specifically, a square lattice exhibits an indirect gap [Fig. 1(a)], with the upper edge of the gap occurring at the corner (M point) of the first Brillouin zone and the lower edge at the X point of the second band [Fig. 1(b)]. When such a square lattice is nonlinear and has a complete gap, a narrow beam propagating in the lattice can induce a localized defect, thereby creating defect states residing in the gap of the transmission spectrum. When the beam inducing such a defect in the lattice has the same wave function as a defect state of the defect it induces, this wave packet self-localizes, becoming a lattice soliton when the self-localized state is stable.[17]

All 2D lattice solitons studied thus far[9–16] have originated from the first band. Here, we find vortex lattice solitons arising from the second band and associated with the four X symmetry points [$k_x = \pi/D$, $k_y = 0$, etc., with D being the lattice spacing; Fig. 1(a)]. Such a soliton can be viewed as a superposition of two degenerate (same β) modes of the induced defect that arises from the second band: one associated with the X point ($k_x = \pm\pi/D$ and $k_y = 0$) and the other associated with the X' point ($k_x = 0$ and $k_y = \pm\pi/D$, which is a 90°-rotated version of the former) with a $\pi/2$ phase delay. In a square lattice, modes arising from the second-band X point have a wave function (to the leading Fourier form in x) of the term $\psi \propto g(x, y)\sin(\pi x/D)f(y)$, where $g(x, y)$ is a positive exponentially decaying function and $f(y)$ is a positive function with periodicity D. Adding an X mode and a $\pi/2$-phase-delayed X' mode yields a new mode proportional to $\sin(\pi x/D) + i\sin(\pi y/D)$, which can be expanded about its zeros as $\psi(x_n + \Delta x, y_m + \Delta y) \propto (-1)^n[\Delta x + i\Delta y(-1)^{m-n}] \propto \exp[i(-1)^{m-n}\theta]$ (with θ being an angle around the expansion points), displaying the phase structure of a 2D array of vortices with alternating rotation between neighboring sites [Fig. 1(c)]. (This expression is a good approximation for β close to the second-band edge; the phase structure deviates from the perfect array of counterrotating vortices as β goes deeper into the gap.)

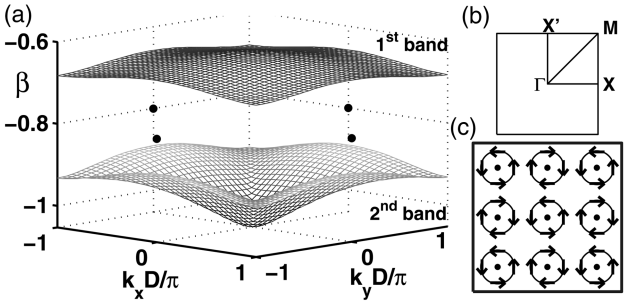

Fig. 1. (a) First two bands of the transmission spectrum in a 2D square lattice with $D = 10$. (b) High-symmetry points of the reciprocal lattice. (c) Phase structure of a counterrotating vortex array, with arrows showing the direction of increasing phase in each vortex.

0146-9592/04/172049-03$15.00/0

Second-band lattice solitons are generic to all nonlinear 2D lattices with a complete gap. As an example, consider the optically induced lattice in Ref. 14. The paraxial dynamics of a linearly polarized beam propagating in such a lattice can be approximated by the dimensionless equation[8,13]

$$i\frac{\partial\psi}{\partial z} + \nabla_\perp^2\psi + \frac{-1}{1+V(x,y)+I}\psi = 0, \qquad (1)$$

where $\nabla_\perp^2 = \partial_x^2 + \partial_y^2$, $V = V_0\{\cos[\pi(x+y)/D] + \cos[\pi(x-y)/D]\}^2$ is the square (induced) lattice[14] and ψ is the slowly varying amplitude of the field. V_0 is the modulation depth of the lattice, and $I = |\psi|^2$ is the soliton intensity, both in units of the background irradiance. For typical experimental values (wavelength $\lambda = 0.5$ μm, linear refractive index $n = 2.3$, relevant electro-optic coefficient $r_{33} = 1340$ pm/V, and applied field of 250 V/mm), one z unit corresponds to $\approx$39 μm, and one transverse (x or y) unit corresponds to $\approx$0.8 μm. For the specific case studied below, the lattice spacing is $D \cong 13$ μm.

We seek stationary solutions of the form $\psi = u(x,y)\exp(i\beta z)$ and find $u(x,y)$ by solving the correspofnding eigenvalue equation by use of self-consistency.[17] Typical results are shown in Fig. 2. The amplitude (absolute value) of this X-point second-band soliton is a ring around the central site, having four weaker rings around it [Fig. 2(a)]. Its phase is an array of counterrotating vortices [Figs. 2(b)]. The central vortex is centered on the central waveguide, and the surrounding vortices have their singularities in adjacent waveguides. The field of this soliton has a singularity in every waveguide it populates, with the phases in adjacent sites rotating in opposite directions [as in Fig. 1(c)].

We simulate the propagation and the stability (in the presence of noise) of these X-point second-band lattice solitons by use of a standard beam propagation method. Typical results are shown in Fig. 2, depicting the amplitude [Fig. 2(a)] and phase [Fig. 2(b)] of an input field (at $z = 0$), the linear diffraction pattern (nonlinearity off) after 100 z units (approximately one diffraction length L_D) [Fig. 2(c)], and the self-trapped output after 100 L_D with an appropriate nonlinearity [Fig. 2(d)]. Note that these modes diffract primarily along the lattice axes, unlike modes residing in the first band. At low amplitudes the soliton extends over several sites, and its propagation constant β is close to the second band edge [Fig. 2(e)]. As the amplitude of the soliton is increased, its wave function is more localized, and its β approaches the lower edge of the first band, eventually becoming a single-site soliton. These second-band vortex lattice solitons do not exist below a threshold power[8] [Fig. 2(e)]. We identify, through simulations, three stability regions for this second-band vortex lattice soliton. For shallow lattices ($V_0 \ll 1$) the soliton is unstable. For lattices with moderate depths ($V_0 \approx 1$) and for a range of moderate soliton amplitudes ($|\psi_{\max}|^2 \approx 0.5$), the soliton is stable. The stable soliton in Figs. 2(a) and 2(b) is marked on the graph in Fig. 2(e) by a dot. For deeper lattices the soliton is unstable. In both its instability regimes, at high peak intensities, the second-band vortex breaks up due to azimuthal instability. It transforms into a rotating dipole structure that loses power and angular momentum as it propagates, rotating more and more rapidly until its poles merge into a stable first-band lattice soliton with zero topological charge. The existence of a stability region for these second-band vortex ring lattice solitons is in direct contrast with vortex ring structures in homogeneous nonlinear media, in which they always undergo azimuthal instabilities.[18]

Next, we find composite multiband solitons made up of two components (with a logic similar to that in Refs. 17 and 19), the first associated with the Γ point of the first band [Fig. 1(b)] and having a bell-shaped structure [Fig. 3(a)], whereas the second has the amplitude and phase structure of the second-band vortex lattice soliton in Figs. 3(b) and 3(c). We find that these composite solitons are stable in the regime in which a scalar soliton made of the dominant component is stable. Namely, if the composite soliton is such that the second-band component is dominant, the composite soliton is stable when the scalar second-band soliton is stable. The same logic applies when the first-band component is dominant. The composite soliton is also stable when the intensities of the components are comparable, in regimes in which a scalar soliton made of either one of the individual components is stable. This is the most interesting regime of composite solitons, because each of the components diffracts when launched individually. In exploring the stability of such composite lattice solitons, we also studied regimes in which the scalar second-band soliton is unstable. It is in this instability regime, and when the intensities of the components are comparable, that we find intriguing new effects. The composite entity disintegrates within $z \approx 100$ (1 L_D) while exchanging angular momentum between its constituents, eventually stabilizing into another form

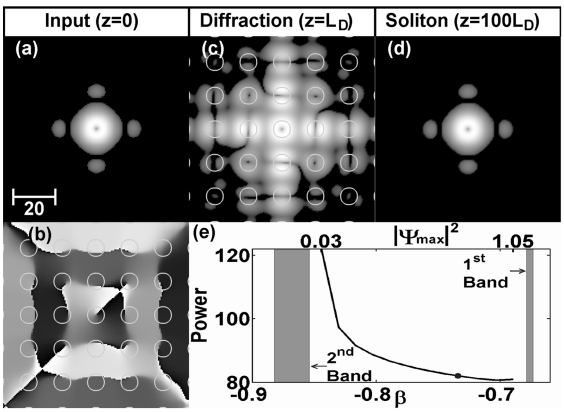

Fig. 2. (a), (b) Intensity and phase of a scalar second-band vortex lattice soliton. (c) Linear diffraction after $z = 100$. (d) Intensity after propagation of $z = 10,000$. (e) Total power of the soliton as a function of the propagation constant and peak soliton intensity for $D = 16$ and $V_0 = 1.1$. The dot represents the soliton shown in (a) and (b). The white circles in (b) and (c) indicate the waveguide boundaries.

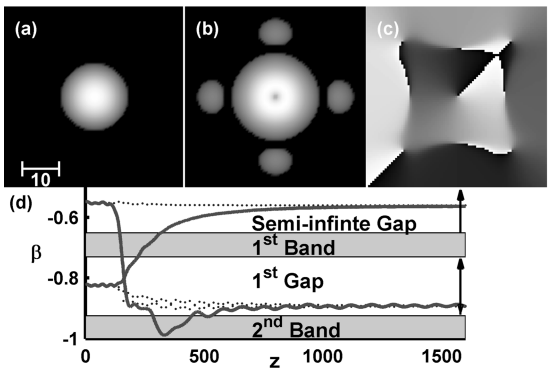

Fig. 3. Vector soliton: (a) intensity of first-band component and (b), (c) intensity and phase of the vortex component arising from the second band. (d) Evolution of the propagation constants of the two components (solid curves), and the propagation constants of the induced defect modes (dotted curves). When the composite entity destabilizes, its second (initially second-band) component transforms into a scalar first-band lattice soliton, whereas its first (initially first-band) component becomes localized by the defect induced by the second component.

of composite soliton. Initially, the first-band component has zero angular momentum (its phase is uniform), whereas the second-band component carries angular momentum and has the complex vortex array shown in Fig. 2(b). As the composite entity becomes unstable, there is a complete metamorphosis: The first-band component acquires angular momentum (transferred from the second component) and the phase structure of a counterrotating vortex array, whereas its amplitude transforms from a bell shape into a ring. Simultaneously, the second-band component undergoes the opposite transformation, losing angular momentum and transforming from a ring into a uniform-phase bell-shaped structure. To understand this process, we estimate the evolving propagation constant of each component and calculate the eigenmodes of the system dynamically while the waves propagate. The evolving propagation constant $\overline{\beta}$ is estimated through an intensity-weighted average of $\beta(x, y) = -(i/\Delta z)\ln[\psi(x, y, z + \Delta z)/\psi(x, y, z)]$, where Δz is the propagation step in the beam propagation method. The results are shown in Fig. 3(d). After $z \approx 100$, the second-band component undergoes azimuthal symmetry breaking, which causes this component to rotate, giving rise to rotation of the first component as well. This moves $\overline{\beta}_1$ (of the first component) toward the second band and $\overline{\beta}_2$ toward the first band. In this process most of the angular momentum of the second component is lost, yet part of it is transferred to the first component. The first component, which started at the semi-infinite gap above the first band, penetrates into the second band, then loses energy by coupling to the modes of the second band, finally stabilizing as an excitation of a localized mode in the gap between the first and the second bands. When that happens, the second component stabilizes as a lattice soliton in the semi-infinite gap and has a structure (amplitude and phase) similar to that initially had by the first component.

In conclusion, we have presented new types of 2D lattice solitons: scalar and composite second-band vortex solitons that have the phase structure of a counterrotating vortex array. These structures can be experimentally realized by exciting two dipole modes with a $\pi/2$ relative phase or by reducing the spatial size (increasing the k-spectrum) of the input vortex beam used in Refs. 4 and 5. The ideas presented here could be implemented in 2D nonlinear photonic lattices, Bose–Einstein condensates, and any other nonlinear periodic system of dimensionality 2 or higher.

This work was supported by the German–Israeli DIP Project, the Israel–USA Binational Science Foundation, the Israeli Science Foundation, and the Ministry of Science, Israel.

References

1. D. N. Christodoulides, F. Lederer, and Y. Silberberg, Nature **424,** 817 (2003).
2. D. N. Christodoulides and R. I. Joseph, Opt. Lett. **13,** 794 (1988).
3. H. Eisenberg, Y. Silberberg, R. Morandotti, A. Boyd, and J. Aitchison, Phys. Rev. Lett. **81,** 3383 (1998).
4. J. W. Fleischer, T. Carmon, M. Segev, N. K. Efremidis, and D. N. Christodoulides, Phys. Rev. Lett. **90,** 023902 (2003).
5. D. Neshev, E. Ostrovskaya, Yu. S. Kivshar, and W. Krolikowski, Opt. Lett. **28,** 710 (2003).
6. D. Mandelik, H. S. Eisenberg, Y. Silberberg, R. Morandotti, and J. S. Aitchison, Phys. Rev. Lett. **90,** 053902 (2003).
7. J. Meier, J. Hudock, D. N. Christodoulides, G. Stegeman, Y. Silberberg, R. Morandotti, and J. S. Aitchison, Phys. Rev. Lett. **91,** 143907 (2003).
8. N. K. Efremidis, J. Hudock, D. N. Christodoulides, J. W. Fleischer, O. Cohen, and M. Segev, Phys. Rev. Lett. **91,** 213906 (2003).
9. B. A. Malomed and P. G. Kevrekidis, Phys. Rev. E **64,** 026601 (2001).
10. J. Yang and Z. H. Musslimani, Opt. Lett. **28,** 2094 (2003).
11. E. A. Ostrovskaya and Y. S. Kivshar, Opt. Express **12,** 19 (2004), http://www.opticsexpress.org.
12. J. Hudock, P. G. Kevrekidis, B. A. Malomed, and D. N. Christodoulides, Phys. Rev. E **67,** 056618 (2003).
13. N. Efremidis, S. Sears, D. N. Christodoulides, J. W. Fleischer, and M. Segev, Phys. Rev. E **66,** 046602 (2002).
14. J. W. Fleischer, M. Segev, N. K. Efremidis, and D. N. Christodoulides, Nature **422,** 147 (2003).
15. J. W. Fleischer, G. Bartal, O. Chen, O. Manela, M. Segev, J. Hudock, and D. N. Christodoulides, Phys. Rev. Lett. **92,** 123904 (2004).
16. D. N. Neshev, T. J. Alexander, E. A. Ostrovskaya, Yu. S. Kivshar, H. Martin, and Z. Chen, Phys. Rev. Lett. **92,** 123903 (2004).
17. O. Cohen, T. Schwartz, J. W. Fleischer, M. Segev, and D. N. Christodoulides, Phys. Rev. Lett. **91,** 113901 (2003).
18. V. I. Kruglov, Y. A. Logvin, and V. M. Volkov, J. Mod. Opt. **39,** 2277 (1992).
19. A. A. Sukhorukov and Yu. S. Kivshar, Phys. Rev. Lett. **91,** 113902 (2003).